UNIVERSIDADE DE SÃO PAULO
Instituto de Física de São Carlos

Proceedings of the seminar to the course

Física Atômica e Molecular

SFI5814 / 2021-2

Ph.W. Courteille (editor)
Universidade de São Paulo
Instituto de Física de São Carlos
13/12/2024

Contents

Preface

Estes anais (ou proceedings) reúnem as monografias elaboradas pelos alunos do curso de Física Atômica e Molecular (SFI5814), realizado no Instituto de Física de São Carlos da Universidade de São Paulo durante o segundo semestre de 2021 sob supervisão do Prof. Ph. W. Courteille.

1

Rydberg atoms

Gabriel Belumat

Instituto de Física de São Carlos, Universidade de São Paulo, 13560-970 São Carlos, SP, Brazil

Abstract: Rydberg atoms are quantum objects with unique properties. By exciting an electron to a very high quantum number n, the atom acquires "exaggerated" behaviour, with long-range interactions, long-lived excited states and peculiar wave functions. In this monograph, we will discuss about these quantum objects, briefly present the methods used to excite Rydberg states, discuss the wave function of the hydrogen atom and show its equivalence to the wave function of alkali atoms with a single valence electron. And show an application of Rydberg states in advanced quantum technologies.

1.1 Introduction

Rydberg atoms are excited atoms whose electrons occupy high principal quantum number orbits with high energy levels. In 1890, the Swedish spectroscopist Johannes Rydberg obtained an empirical formula for several frequencies present in the hydrogen spectrum, by attempting to reproduce analytically the frequencies measured in the laboratory.

$$f = R_H \left(\frac{1}{m^2} - \frac{1}{n^2} \right) \tag{1.1}$$

However, as this was before to the development of quantum mechanics, he was unable to explain the formula he had obtained on a more theoretical basis. The explanation would came later with Bohr and Sommerfeld, who quantified the angular momentum of the electron orbits. When in a Rydberg state, the valence electron of alkali atoms has a wave function very similar to that of hydrogen, especially when it is in states of very high angular momentum, called circular states, this is due to the fact that the charges in the nucleus are shielded by the charges of the electrons that are in lower energy states, so that the electron that is in a Rydberg state mostly feels a Columbian potential identical to that of the hydrogen atom. This explains why the Rydberg formula applies to a wide range of atoms in states with high principal quantum numbers.

Today, Rydberg atoms are widely implemented in various quantum systems, being used in sensors due to their sensitivity to electric and magnetic fields, producing sensors capable of detecting minimal changes in the environment [12], as well as in areas of quantum computing [11] and nonlinear optics, as mediators of interactions between photons [13].

1.2 Excitation of Rydberg states

To produce Rydberg atoms, it is necessary to use processes that can transfer a significant amount of energy to the electronic layer of the atom, but without ionising it. Three different techniques have been used throughout history: electron impact, charge exchange and photoexcitation. These three techniques are briefly discussed in [1].

1.2.1 Eletron Impact Excitation

$$e^- + A \rightarrow A \;\; nl + e^- \tag{1.2}$$

This first method simply consists of bombarding a rarefied gas with an electron beam,the collision between the electron beam and the atoms of the gas can transfer sufficient energy to the eletrons of the atoms [Figure 1.1], producing a spectrum of excited states along with ionised atoms. The ions formed can be easily trapped by applying an electric potential within the gas chamber. In this way, it is possible to produce a beam of atoms with atoms in different Rydberg states along with other states.

This technique is much simpler than others because electron beams are easy to produce, and it has been possible to control the energy of the electrons in various ways, such as using a magnetic field.

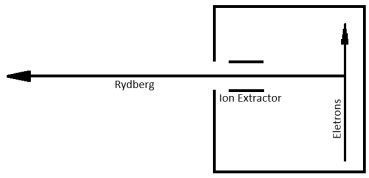

Figure 1.1: Symplified experimental system to create a atomic beam with Rydberg atoms using eletron colisions.

However, the technique has low selectivity in terms of which states are excited, and even by controlling the energy of the electrons, there is no way of predicting which energy will be transferred to the atom in a collision process.

1.2.2 Charge Exchange Excitation

$$A^+ + B \rightarrow A \;\; nl + B^+ \tag{1.3}$$

In this process, a chamber containing a rare gas is bombarded with a beam of ions [Figure 1.2. Inside the chamber, the ions can capture the electron of a neutral atom with an energy greater than that of the ground state. We then need to separate the remaining ions by applying an electrical potential that will deflects the ions from their original trajectory.

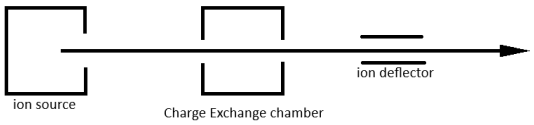

Figure 1.2: Symplified experimental system to create a atomic beam with Rydberg atoms using charging exchange of ions.

As with the other processes, the low efficiency in producing Rydberg states is also a problem, as the fraction of Rydberg atoms produced compared to the number of ions is very low, for states with n=10, this fraction is about 10^{-3} [1]. We can think that this problem is easily solved by improving the size of the gas chamber, but this also improves the scattering by the neutral atoms from the chamber, resulting in more losses.

1.2.3 Optical Excitation

$$hf + A \rightarrow A \;\; nl \tag{1.4}$$

The excitation of Rydberg states by optical excitation has a crucial difference when compared to the other two processes: it is possible to select the Rydberg state created, by selecting the photon energy. It consists in transferring the energy of a photon to the electron in the atom, thus creating a specific state. However, the difficulty of this process, lies in the technological challenge of creating lasers with the necessary wavelengths. However, the development of lasers with the right frequencies has played an important role in Rydberg atoms research.

1.3 Eletron Wave funcion

When working with quantum objects, we are always looking for a way to describe the system algebraically, with a wave function or some state notation. To analyze some effects and properties of Rydberg atoms, one must first is to look for a wave function that can describe the electron in a Rydberg state.

For this task, we will use the quantum defect method, which is a good approximation for atoms with a single valence electron, including the hydrogen atom. The valence electron dynamics of a hydrogen atom in a Rydberg state and an electron from an element such as sodium (Na) in a Rydberg state are very similar. For Na, the valence electron in a Rydberg state, sees the nucleus as having only one unit of charge, since the rest of the electrons are shielded by the rest of the electrons, but only valid for the part of the wave function that is significantly away from the nucleus, if we consider a state with high ellipticity, that is, a state with low angular momentum, part of the wave function may be within the shielding of the other electrons in the electrosphere, causing a loss of energy that can be expressed as:

$$W = \frac{-R_y}{(n-\delta_l)^2} \tag{1.5}$$

Where δ_l is an empirically observed quantum defect for orbitals of angular momentum l. The energy differences between a Na atom and a hydrogen atom are clearer for states with low angular momentum, for states with high l, this difference becomes negligible, such a similarity facilitates our understanding of the properties of Rydberg atoms , since the wave functions of the hydrogen atom are well known. To

begin our description, let's start with the Hamiltonian of hydrogen, given by:

$$\left(-\frac{\nabla^2}{2}-\frac{1}{r}\right)\psi = W\psi \tag{1.6}$$

This is also true for valence electrons far from the ionic nucleus, which feel only one unit of charge. As already known for hydrogen, the wave function can be written as the product of the angular and radial solutions, with the angular part written as normalized spherical harmonics of the form:

$$Y_{lm}(\theta,\phi) = \sqrt{\frac{(l-m)!}{(l+m)!}\frac{2l+1}{4\pi}} P_l^m(cos\ \theta)\ e^{im\phi} \tag{1.7}$$

Where l is the angular momentum projected in the quantization axis, and can be zero or a positive integer, m is the magnetic quantum number and goes from $-l$ to l. But the interesting part is the radial part, where we can see the differences between the atoms. The equation for the radial part can be written as:

$$\frac{\partial^2\rho}{\partial r^2} + \left[2W + \frac{2}{r} - \frac{l(l+1)}{r^2}\right]\rho = 0 \tag{1.8}$$

Where, by definition $R(r) = \frac{\rho(r)}{r}$. This equation is the Coulomb radial equation, and has two solutions, a regular one ($f(W,l,r)$) and an irregular one ($g(W,l,r)$). Given the boundary conditions $\psi \to 0$ for $r \to 0$ and $r \to \infty$, only the regular solutions are allowed. For $r \to 0$, the solution behaves like $f \propto r^{l+1}$. Considering $W < 0$, we can introduce an effective quantum number β defined by $W = -\frac{1}{2\beta^2}$. For $r \to \infty$, the solution f can be expressed as increasing and decreasing exponential functions $u(\beta,l,r)$ and $v(\beta,l,r)$ [2], where f is given by:

$$f \to u(\beta,l,r)\ sin\ \pi\beta\ -\ v(\beta,l,r)e^{i\pi\beta} \tag{1.9}$$

Looking again at the boundary condition $\psi \to 0$ for $r \to \infty$, it is possible to notice that we need to β to be an integer n, thus recovering the hydrogen allowed energies $W = -\frac{1}{2n^2}$. It is possible now possible to use quantum defect theory [1], to find an approximation for the wavefunction of atoms with a single valence electron. Changing the potential $-1/r$ of the hydrogen atom for the effective potential $V_{eff}(r)$ of an ionic spherical nucleus, the only notable difference is found in the radial equation. Points with lower r, interacting with the nuclei of the atom, see a larger charge. In the points far from the nucleus, is not possible to distinguish the potential of a Coulomb potential. Thus, the effect observed in the external wave function is just a change in the phase relative to the hydrogen atom [Figure 1.4]. For a s electron, the phase shift relative to H can be expressed as:

$$\tau = \int_0^{r_0} \left\{ [W - V_{eff}(r)]^{\frac{1}{2}} - \left[W + \frac{1}{r}\right]^{\frac{1}{2}} \right\} \sqrt{2}\ dr \tag{1.10}$$

For regimes where $|W| << 1/r_0$, it is possible to extend this expression in power series and take only the first order::

$$\tau = \int_0^{r_0} V_d(r) \left(\frac{r}{2}\right)^{\frac{1}{2}}\ \ dr. \tag{1.11}$$

Where $V_d(R)$ is defined as $V_d = -\ 1/r - V_{eff}$. Thus, the pure f radial solution of the hydrogen wave function is replaced by:

$$\rho(r) = f(W,l,r)\ cos\ \tau - g(W,l,r)\ sin\ \tau, \tag{1.12}$$

Where $g(W,l,r)$ is the irregular solution of the Coulomb equation. This leads to a change of the effective principal quantum number β defined in 2.8. Considering the boundary conditions, we get $\beta = n - \tau/\pi$, where τ/π is the quantum defect δ_l. Then, the wave function for a single valence electron, with large radius states, can be written as:

$$\psi = \frac{Y_{lm}[f(W,l,r)\ cos\ \pi\delta_l - g(W,l,r)\ sin\ \pi\delta_l]}{r}. \tag{1.13}$$

Which has the allowed energies:

$$W = -\frac{1}{2(n-\delta_l)^2}. \tag{1.14}$$

These energies have already been introduced in equation 2.4, and the constant δ_l describes the difference between the energies of the single valence electrons, and the hydrogen electron. For states such as the circular states, which will be briefly discussed next, the probability of the electron being encontered at $r < r_0$ is too small, that way, so the energy dumping became very small.

1.4 Quantum Technologies

Due to some characteristics of Rydberg states, such as long-range dipole-dipole interactions, long-lived states, high coupling to external fields, Rydberg atoms are widely used in the development

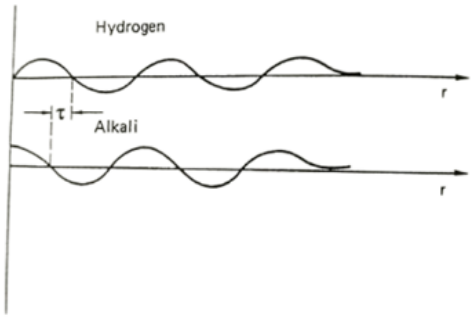

Figure 1.3: Behavior of the electron wave function of an alkali atom and a hydrogen atom. The alkali electron aquires a phase τ due to its interaction with the potential of the ionic nucleus.

of quantum technologies. Platforms using Rydberg atoms can be used as versatile quantum simulators, enabling the simulation of many-body systems [3], in addition to being a promising platform for the implementation of quantum computing algorithms [4].

1.4.1 Quantum processor

One of the biggest problems with quantum computing is the low fidelity of the systems, which leads to data loss during processing. To get around this,classical computing uses error correction algorithms that can make copies of the processed data to ensure fidelity at the end of processing, but in quantum systems it is not possible to make a copy of quantum states due to the no cloning theorem [10]. What can be done is to use quantum entanglement to increase the fidelity of the systems.

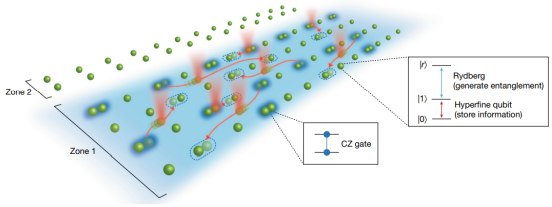

Figure 1.4: Schematic drawing of the experiment, in which atoms are moved in a two-dimensional network, using optical tweezers, in this way, it is possible to create quantum logic gates (zone 1). To increase the fidelity of the system, another set of atoms (zone 2) is used for an error correction algorithm using quantum entanglement. Image from [9]

In [9], an experimental setup is shown that uses optical tweezers to move atoms in a two-dimensional network, while exciting the atoms in a Rydberg state and in a clock state, the clock state of the atoms is used to store the information generated by the qubit, while the Rydberg state is used to generate entanglement between the atoms used for processing and the atoms used for error correction, thus increasing the fidelity of the processor, a very important advance for quantum computing.

1.5 Conclusion

Rydberg atoms proved to be very interesting objects to study, with a wide range of applications and peculiar properties. In an attempt to better understand the electronic function in Rydberg states, the similarity of the wave functions for an alkali atom and a hydrogen atom was shown, a result that I find surprising, given the complexity of atomic systems with many electrons. The quantum deffect theory approximation is able to make reasonable corrections even for Rydberg states with higher ellipticity.

It was still possible to briefly discuss a quantum technology under development, that uses the concept of Rydberg states in the context of quantum computing, using such states to generate long-range entanglement and applying error correction algorithms to increase the fidelity of the systems used for quantum processing.

Bibliografia

[1] Thomas F. Gallengher *Rydberg Atoms* (2005), Cambridge University Press.

[2] M J Seaton *Quantum Defect Theory* (1983), Cambridge University Press, Rep. Prog. Phys. **46**.

[3] J. Zeiher, J.-y. Choi, A. Rubio-Abadal, T. Pohl, R. van Bijnen, I. Bloch, and C. Gross *Coherent Many-Body Spin Dynamics in a Long-Range Interacting Ising Chain* (2017), Phys. Rev. X **7**, 041063.

[4] L. Isenhower, E. Urban, X. L. Zhang, A. T. Gill, T. Henage, T. A. Johnson, T. G. Walker, and M. Saffman, *Demonstration of a Neutral Atom Controlled-NOT Quantum Gate* (2010), Phys. Rev. Lett. **104**.

[5] R. G. Hulet and D. Kleppner, *Rydberg Atoms in 'Circular' States* (1983), Phys. Rev. Lett. **51**, 16.

[6] Andrea Muni, Léa Lachaud, Angelo Couto, Michel Poirier, Raul Celistrino Teixeira, Jean-Michel Raimond, Michel Brune and Sébastien Gleyzes, *Optical coherent manipulation of alkaline-earth circular Rydberg states* (2022), Nature Physics **18**, 502.

[7] R. C. Teixeira, A. Larrouy, A. Muni, L. Lachaud, J.-M. Raimond, S. Gleyzes, and M. Brune, *Preparation of Long-Lived, Non-Autoionizing Circular Rydberg States of Strontium* (2020), Phys. Rev. Lett. **125**, 263001.

[8] C. Hölzl , A. Götzelmann , E. Pultinevicius , M. Wirth , and F. Meinert, *Long-Lived Circular Rydberg Qubits of Alkaline-Earth Atoms in Optical Tweezers* (2024), Phys. Rev. X **14**, 021024.

[9] D. Bluvstein, H. Levine, G. Semeghini, T. T. Wang, S. Ebadi, M. Kalinowski, A. Keesling, N. Maskara, H. Pichler, M. Greiner, V. Vuletić and M. D. Lukin, *A quantum processor based on coherent transport of entangled atom arrays* (2022), Nature **604**, 451.

[10] J. Park, *The concept of transition in quantum mechanics* (1970), Foundations of Physics **1**, 23.

[11] S. R. Cohen, Jeff D. Thompson, *Quantum Computing with Circular Rydberg Atoms* (2021), Phys. Rev. X Quantum **2**, 030322.

[12] H. Fan, S. Kumar, J. Sedlacek, H. Kübler, S. Karimkashi and J. P Shaffer, *Atom based RF electric field sensing* (2015), J. Phys. B: At. Mol. Opt. Phys. **48**.

[13] M. Moreno-Cardoner, D. Goncalves, and D. E. Chang, *Quantum Nonlinear Optics Based on Two-Dimensional Rydberg Atom Arrays* (2021), Phys. Rev. Lett. **127**, 263602.

2

Schrödinger cats

João V. B. de S. Merenda

Instituto de Física de São Carlos, Universidade de São Paulo, 13560-970 São Carlos, SP, Brazil

Abstract: Quantum mechanics, developed in the early 20th century, revolutionized our understanding of the microscopic world. Schrödinger proposed his famous experiment in 1935 to question the implications of these quantum peculiarities on macroscopic objects, exemplified by a cat that exists in a paradoxical state of being both alive and dead. This work explores Schrödinger's cat, a thought experiment that illustrates quantum mechanics' peculiarities, challenging traditional interpretations of reality. Laboratory experiments inspired by Schrödinger's cat, including photon entanglement and ion superposition, are discussed, highlighting key advances in recreating "cat states" under controlled conditions.

2.1 Introduction

In the early 20th century, the rise of quantum mechanics revolutionized our understanding of the microscopic world. Unlike classical physics, which describes a predictable, well-defined reality, quantum mechanics is inherently probabilistic: particles can exist in multiple states simultaneously, a phenomenon called superposition, until they are observed. This shift raised fundamental questions about the nature of reality: if particles can be in several states at once, what does this imply for our understanding of the physical world?

There are three primary perspectives about the inderteminancy of quantum mechanics:

The **Realist** Position, led by Einstein in the EPR paradox [1], holds that nature is entirely objective. Any measurement uncertainty arises from incomplete information or hidden variables, rather than an intrinsic indeterminacy. From this perspective, quantum mechanics is seen as an incomplete description of nature.

The **Orthodox** (or **Copenhagen**) Interpretation contends that quantum mechanics is a complete theory, but that certain aspects of quantum reality inherently prevent a fully deterministic description.

The **Agnostic** Position suggests that the true state of a system between its creation and measurement cannot be experimentally verified, making it impossible to definitively ascertain the nature of the microscopic world.

To illustrate the paradox of quantum mechanics, physicist Erwin Schrödinger proposed his famous thought experiment, "Schrödinger's Cat" in 1935. He envisioned a cat in a sealed box, its life or death dependent on a probabilistic event. Until observed, the cat is simultaneously alive and dead, an idea that sharply contrasts with our everyday experience of reality and highlights the strangeness of quantum mechanics.

In the sections that follow, we will explore key concepts: Section 2.2 introduces the basics of the Copenhagen interpretation of quantum mechanics; Section 2.3 explains Schrödinger's cat experiment; Section 2.4 shows the mathematical formulation of the Schrödinger's cat state; Section 2.5 examines real-world laboratory experiments inspired by Schrödinger's cat; and Section 2.6 considers the implications for quantum computing.

2.2 Basic Concepts

Non-relativistic quantum dynamics is governed by Schrödinger's equation (2.1), which describes the time evolution of a quantum system.

$$\hat{H}|\Psi\rangle = i\hbar\frac{\partial}{\partial t}|\Psi\rangle \tag{2.1}$$

This linear differential equation has either a discrete or continuous set of solutions. For clarity, we will focus on the discrete case, noting that all concepts can be extended to the continuous case. Below, we will define the pillars of the Copenhagen

interpretation, established by Niels Bohr, Werner Heisenberg, Max Born, and others.

1. **The superposition principle**: Due to the linearity of Equation (2.1), any state of the system can be expressed as a linear combination of the system's eigenstates:

$$|\Psi(x,t)\rangle = \sum_n c_n |\psi(x)\rangle e^{-iE_n t/\hbar} \tag{2.2}$$

   The wave function $|\Psi(x,t)\rangle$ provides complete information about the system, encapsulating all possible states, each of which evolves simultaneously over time.

2. **The statistical interpretation**: Max Born emphasized the fundamentally probabilistic nature of quantum mechanics. The wave function itself encodes probabilities: the square of its module gives the probability of finding the system in a particular state. Each coefficient c_n in the wave function represents a probability amplitude for a specific state, and these amplitudes must be normalized, as shown in equation (2.3), to ensure that the total probability across all possible states is 1.

$$||\Psi||^2 = \sum_n |c_n|^2 = 1 \tag{2.3}$$

3. **Observables**: In quantum mechanics, measurements of a system are represented by Hermitian operators, which represents **observables** measures, such as energy, momentum, postition. Each Hermitian operator is associated with a set of eigenstates:

$$\hat{A} : \mathcal{H} \to \mathcal{H} \Rightarrow \hat{A}|\psi\rangle = a_n|\psi\rangle \tag{2.4}$$

The concepts above, along with the measurement paradox discussed below, form the basis of the Copenhagen interpretation [2, 3, 4].

2.2.1 Quantum measurements

The measurement problem plays a central role in quantum theory. In classical physics, a system is fully described by a complete set of measurable physical quantities, each with well-defined values [2]. In quantum mechanics, however, only a specific set of observables can be measured, and these observables are subject to intrinsic limitations. Not all properties can be simultaneously measured with precision, as highlighted by the Uncertainty Principle. This distinction raises fundamental questions about the nature of reality and measurement in quantum systems.

The measurement problem, or measurement paradox, was first examined by John von Neumann in his book *Mathematical Foundations of Quantum Mechanics* [5]. Von Neumann proposed that the measurement apparatus projects the operator $\hat{A}$ onto an eigenvector basis, producing a distribution of probability amplitudes for the possible outcomes as shown in equation (2.5). Subsequently, when the scientist observes the result, the system is reduced to a single possible state, effectively collapsing the wave function. This effect is known as wave function collapse or wave function reduction.

$$\langle \hat{A} \rangle = \sum_k a_k |c_k|^2 \tag{2.5}$$

The Copenhagen school argued that a classical apparatus is essential to collapse the wave function, as described by von Neumann. However, there is no clear way to define the precise boundary between the quantum and classical realms in nature's description.

2.3 The Schrodinger's Cat as a thought experiment

In response to the EPR paradox (see section 2.1) and the peculiar nature of quantum measurements, Erwin Schrödinger proposed the famous thought experiment known as **Schrödinger's cat** in 1935 [6].

Imagine a cat placed inside a sealed box along with a mechanism triggered by the decay of a radioactive atom. If nuclear decay occurs, the device releases poison, killing the cat. However, the box is completely sealed, so no external observer can determine the cat's state until they open the box. Since atomic decay is a probabilistic event, quantum mechanics suggests that, until observed, the atom exists in a superposition, both decayed and undecayed simultaneously. This implies that the cat, a macroscopic object, is also in a superposition, being both alive and dead at the same time, as shown in (2.6), a scenario clearly impossible in the classical world.

$$|\Psi_{cat}\rangle = \frac{1}{\sqrt{2}}(|\Psi_{alive}\rangle + |\Psi_{dead}\rangle) \tag{2.6}$$

Schrödinger's point was to show how strange and counterintuitive quantum superposition is when applied to real-life objects, highlighting the disconnect between the quantum and macroscopic worlds.

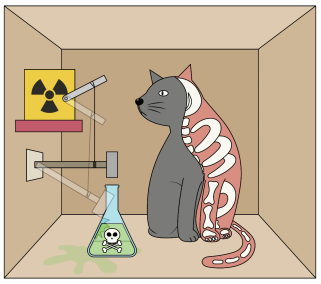

Figure 2.1: A conceptual diagram illustrating Schrödinger's cat thought experiment, where the cat is simultaneously alive and dead until an observation is made.

2.4 Cat's state

We can describe the light in quantum mechanics into two difrerent ways: using the photon number $|n\rangle$, also known as Fock states, or using coherent (or Glauber) states $|\alpha\rangle$. In practice terms, we can express the coherent states in terms of the Fock states:

$$|\alpha\rangle = e^{|\alpha|^2/2} \sum_{n=0}^{\infty} \frac{\alpha^n}{\sqrt{n!}} |n\rangle \tag{2.7}$$

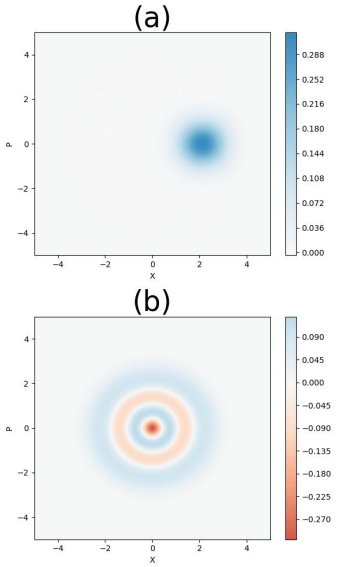

Figure 2.2: (a) Wigner function of a coherent state with $\alpha = 1.5$, showing near-classical behavior. (b) Wigner function of a Fock state with $n = 3$, highlighting purely quantum characteristics.

Figure 2.2 illustrates the Wigner functions of Fock and coherent states. Fock states exhibit purely quantum behavior. In contrast, coherent states, while still fundamentally quantum, are as close to classical behavior as possible. As the photon number $|n\rangle$ increases in the Equation (2.7), the uncertainty in the system decreases, resulting in a state that appears increasingly classical.

Now, consider a system in a pure state (or superposition) of two opposite coherent states, as shown in equation (2.8). This state can also be represented by a density matrix, as in equation (2.9), which corresponds to what is known as a "cat state." In this matrix, the diagonal terms represent the populations, while the off-diagonal terms correspond to the coherence between states. Figure 2.3(a) displays the Wigner function of the cat state, highlighting the interference pattern between the two peaks.

$$|\Psi_{cat}\rangle = \frac{1}{\sqrt{2}}(|\alpha\rangle + |-\alpha\rangle) \tag{2.8}$$

$$\rho_{cat} = \frac{1}{2}((|\alpha\rangle + |-\alpha\rangle)(\langle\alpha| + \langle-\alpha|)) \tag{2.9}$$

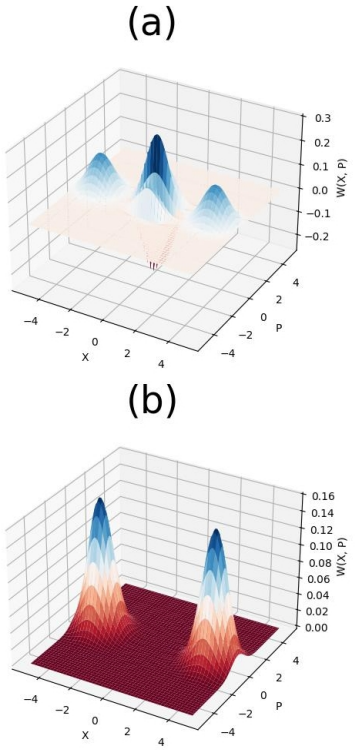

Figure 2.3: (a) Wigner function representing a 'cat state,' a superposition of two opposite coherent states. (b) Wigner function of the same system after decoherence, showing the loss of quantum coherence and a shift towards a classical mixture.

However, interaction with the environment causes decoherence, which destroys the cat state, transforming it into a statistical mixture, as shown in Figure 2.3(b) [9].

2.5 The Schrodinger's cat in laboratory

Producing Schrödinger's cat states, often called "cat states", in the laboratory is very difficult. Interactions between the system and its environment, also referred to as decoherence, quickly disrupt any attempt to maintain a coherent superposition. However, in this section, we will highlight some successful examples of cat state generation achieved in experimental settings.

2.5.1 Haroche's experiment

The first experiment was conducted by Haroche and collaborators in 1996 [7]. We can divided the experiment into two steps:

1. **Preparation of the cat state:** The experiment utilized circular Rydberg atoms of rubidium, where the outer electron orbits in a large-diameter circle, approximately a thousand times larger than that of a ground-state atom. These states, $|e\rangle$ (with n = 51) and $|g\rangle$ (with n = 50), were prepared using a combination of laser and radiofrequency excitation techniques.

   To create the superposition, a pulse of resonant microwave radiation was applied, mixing the $|e\rangle$ and $|g\rangle$ states in the R1 cavity shown in figure 2.4. This resulted in a coherent superposition where the electron simultaneously occupied the two states, analogous to Schrödinger's cat as shown in equation (2.10). The interference between the states produced a dynamic electric dipole in the atom, behaving like a rotating antenna sensitive to microwave radiation at 51 GHz.

2. **Measurement of the cat state:** The measurement involved detecting the phase shift of the atomic dipole caused by its interaction with the cavity field denoted by C in figure 2.4. This phase shift is influenced by the non-resonant microwave field interacting with the atom, which shifts the atomic energy levels and alters the dipole's rotation frequency. Importantly, this method does not absorb or destroy the photons, maintaining the integrity of the system, a non-destructive measurement.

   The magnitude of the phase shift, which could reach up to 180°, correlated directly with the number of photons in the cavity, effectively allowing for photon counting. This approach ensured the ability to probe the quantum state of the light field while preserving the coherence of the cat state. The measurement of the phase shift occurs in the cavity R2 (see figure 2.4).

   This methodology showcases a precise interaction between Rydberg atoms and the microwave cavity, highlighting the quantum behavior of light and matter.

$$|\Psi\rangle = \frac{1}{\sqrt{2}}(|e, \alpha e^{i\phi}\rangle + |g, \alpha e^{-i\phi}\rangle) \tag{2.10}$$

Where ϕ is the radiation field phase. The experimental apparatus is shown in Figure 2.4

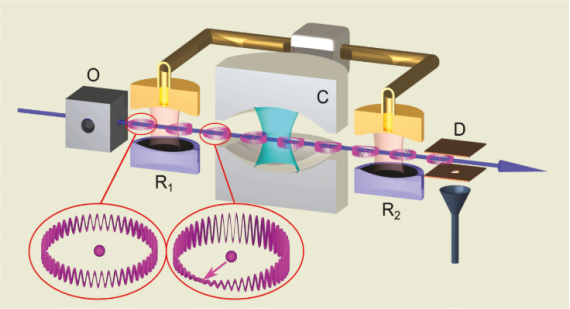

Figure 2.4: Experimental setup of the cavity QED Ramsey interferometer. Insets illustrate the atom in a circular orbit, prepared in an initial energy eigenstate (left) and then in a superposition state after interacting with the microwave field in cavity R1. Font: Haroche, 2013 [8]

After exiting the R2 cavity, the decoherence process begins, gradually causing the system to behave more classically, as illustrated in Figure 2.5. During decoherence, interactions with the environment cause the quantum superposition of states to break down, leading the system toward a state that appears classical. This experiment was fundamentally important for exploring the boundary between classical and quantum mechanics.

2.5.2 Others Schrödinger's cat experiments

In 1999, Arndt and Zeilinger conducted a experiment with large molecules, including C_{60} "buckyballs," revealing interference patterns that confirmed wave-like behavior. This demonstrated superposition in larger, complex molecules, significantly extending the reach of quantum mechanics into more massive systems and challenging traditional boundaries of quantum behavior [10].

In 2005, Wineland's team at NIST created Schrödinger cat states with trapped beryllium ions, showing superpositions in which ions existed in multiple quantum states at once. This experiment explored coherence in atomic superpositions and helped develop techniques for quantum information.

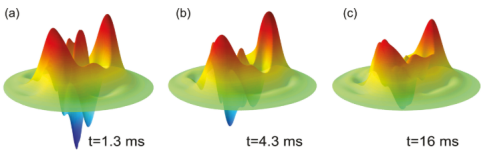

Figure 2.5: The evolution of a Schrödinger cat state as a single atom crosses the cavity, demonstrating decoherence over time: (a) $t = 1.3ms$ (b) $t = 4.3ms$, and (c) $t = 16ms$. As time progresses, the system transitions from quantum superposition to a statistical mixture state. Font: Haroche, 2013 [8]

2.6 Implications for Quantum Computing

Schrödinger's cat plays a fundamental role in quantum computing, quantum information and quantum cryptography. The fundamental unit of information in quantum computing, the qubit, serves a similar role to the classical bit. However, unlike a classical bit, which can exist in one of two distinct states (0 or 1), a qubit can exist in a superposition of both states simultaneously as the Schrödinger's cat (see equation (2.11)). This property allows quantum computers to process vast amounts of information in parallel, offering exponential speedups for certain computational tasks.

Despite this advantage, quantum systems are highly sensitive to external disturbances, a phenomenon known as decoherence. Due to decoherence, the fragile quantum states rapidly lose their coherence and transition to classical behavior if they are not carefully isolated from their environment. This sensitivity to disturbance is one of the most significant challenges in maintaining and scaling quantum computers, as even minor interactions with the environment can collapse the superposition states, effectively reducing computational power.

Known as Bell states when pairs of qubits are perfectly entangled (see equation (2.12)), entanglement allows qubits to perform tasks beyond the capability of classical bits. This quantum correlation enables unique applications, such as quantum teleportation and quantum key distribution in cryptography, where information can be transmitted with theoretically unbreakable security. In quantum computing, entanglement is a key resource for performing quantum logic operations, linking qubits in ways that enhance computational power and enable the execution of complex algorithms like Shor's and Grover's algorithms.

$$|\Psi\rangle = \alpha|0\rangle + \beta|1\rangle \tag{2.11}$$

$$|\psi\rangle = \frac{1}{\sqrt{2}}(|00\rangle + |11\rangle) \tag{2.12}$$

2.7 Conclusion

In the macroscopic world, classical mechanics governs the behavior of objects with certainty and determinism. In contrast, the microscopic world exhibits strange phenomena that challenge our conventional understanding of reality. One of Bohr's postulates, the complementarity principle, suggests that quantum mechanics is a complement to classical mechanics, but the boundary between the two remains unclear. Schrödinger's cat experiment, proposed in 1935, explores the relationship between a probabilistic system (such as radioactive decay) and a macroscopic object of measurement, the cat. This thought experiment helps to shed light on the frontier between quantum and classical realms. However, creating Schrödinger's cat states in the laboratory is challenging due to decoherence, the loss of quantum information to the environment. Despite this, physicists like Haroche and others have successfully generated Schrödinger's cat states in the lab, bringing us closer to understanding the boundary between the quantum and classical worlds.

Bibliografia

[1] A. Einstein, B. Podolski, N. Rosen *Can quantum-mechanical description of physical reality be considered complete?* (1935).

[2] Ph. W. Courteille *Quantum Mechanics applied to Atoms and Light* (2023).

[3] R. L. G. Hughes *The structure and interpretation of quantum mechanics* (1989).

[4] R. Omnés *Interpretation of quantum mechanics* (1987).

[5] J. V. Neumann *Mathematical foundations of quantum mechanics* (2018).

[6] E. Schrödinger *Die gegenwiirtige Situation in der Quantenmechanik.*, Naturwissenschaften, **23** (1935).

[7] S. Haroche *Observing the progressive decoherence of the "meter" in a quantum measurement.*, Physical review letters, **77** (1996).

[8] S. Haroche *Controlling Photons in a Box and Exploring the Quantum to Classical Boundary.* Reviews of Modern Physics, **85** (2013).

[9] W. H. Zurek, *Decoherence and the transition from quantum to classical*, Physics today, **44** (2001).

[10] M. Arndt, A. Zeilinger, *Wave-particle duality of C60 molecules*, Nature, **401** (1999).

3

Supersolids in dipolar shells

Rafael A. R. da Paz

Instituto de Física de São Carlos, Universidade de São Paulo, 13560-970 São Carlos, SP, Brazil

Abstract: The field of dipolar quantum gases has blossomed due to the manifestation of unique effects introduced by dipole-dipole interaction. In these ultracold systems, quantum fluctuations energy can become relevant, which potentially brings to the emergence of simultaneous behavior of solid and superfluid, known as supersolidity. This work reviews the main aspects of the supersolid phase and briefly summarizes key experimental evidence of its occurrence. Restricting us to a thin shell trap, we propose an *ansatz* to build a diagram of phases. Bose-Einstein condensate and isolated droplets domains have been predicted, with the possibility of supersolidity in a narrow region between them. Our findings partially agree with the reference numerical results.

3.1 Introduction

Ultracold gases have been established as a platform to study extreme effects of the quantum nature of matter. The competition between dimensionality, geometry, and the strength of interactions, highly tuned in these systems, raises a myriad of regimes inconceivable before the development of Quantum Mechanics. One of these, Bose-Einstein condensation, requires the lowest temperatures known by humanity, and has been shown as a fertile ground for the appearance of novel physical phenomena. Examples of these occurrences include propagation of distinct modes of sound, vortex dynamics, topological transitions, and the arising of new phases of matter [1, ?, 3].

In particular, dipolar gases polarized by a strong magnetic field present unique signatures. Their interplay of isotropic and short-ranged contact interaction in front of an anisotropic and long-ranged dipole-dipole potential modifies the density pattern. Besides it, confinement provides additional spatial constraints. As a result of this balance, special features can arise, like new arrangements or distinct collective modes [1, 4]. An eccentric trapping consists of thin shells or bubbles, a kind of harmonic oscillator whose minimum is displaced by a finite radial distance from the center of the trap. Applying this potential in an ultracold dipolar gas reveals unrecorded consequences in any other combination of trap and interactions [1].

Recent works have pointed out the quantum fluctuations also should be added to this balance [5, ?]. This energy correction explains why systems previously expected to collapse could be maintained stable for large lifetimes [?, 3, 4, 5]. Additionally, taking into account this term has been useful for theoretically predict dipolar quantum droplets and supersolids [5, ?], exotic phases of matter experimentally recorded [?, 3].

This work describe what is a supersolid and how it can emerge in dipolar ultracold gases as a consequence of quantum fluctuations. It will be supposed the system is initially Bose-Einstein condensed and the text is organized as follows. The Section 3.2 contains the mathematical tools that govern the systems of interest remarking standard Mean Field regime and Beyond Mean Field correction. At this point, the exotic phases of quantum droplets and supersolids are presented in Sections 3.3 and 3.4, respectively. Section 3.5, introduces thin shell trap and cites the occurrence of these phases of matter in this platform. Finally, Section 3.6 brings the findings of our group at IFSC and compares it with the main available theoretical results.

3.2 Background

Bose-Einstein condensates (BECs) are systems characterized by a macroscopic population of a unique microscopic state. As a consequence, this phase of

matter shows properties due exclusively to this only one state. In addition, two remarkable features of BECs are coherence and *Off-Diagonal Long Range Order*. It means all the system behaviors like an individual entity due to the wave character of the atoms [7].

To describe a BEC and the transitions to other phases by tuning of distinct parameters, it should be introduced the extend Gross-Pitaevskii Equation (eGPE)

$$\left[-\frac{\hbar^2}{2m}\nabla^2 + V_{tr}(\vec{r}) + V_{int}(\vec{r}) + \gamma_{QF}|\Psi|^3\right]\Psi(\vec{r},t) = \\ = i\hbar\frac{\partial\Psi}{\partial t}. \tag{3.1}$$

Inside the square brackets, the first term is the kinetic energy, whose contribution is appreciable only for low number of atoms. The second one is the external trap potential, needed in most cases to confine the atoms. Usually, this term has a harmonic form, but recently other geometries like cigar, pancake, cylinder, hollow sphere, and bubble have been employed. The third contribution takes into account the interatomic interaction, i. e., this is an internal potential, in contrast to the last one. In polarized dipolar gases, that term is given by

$$V_{int}(\vec{r}) = g|\Psi|^2 + \frac{1}{2}\int d\tau' \frac{C_{dd}}{4\pi}\frac{1-3cos^2(\theta)}{|\vec{r}-\vec{r'}|^3}|\Psi(\vec{r'},t)|^2, \tag{3.2}$$

where $g = 4\pi\hbar^2 a_s/m$, the contact interaction parameter, depends on the *s-wave scattering length*, $C_{dd} = \mu_0\mu^2$ is related to the magnetic moment of the species, while θ is the angle between the dipole's direction and the relative position vector (see figure 3.1).

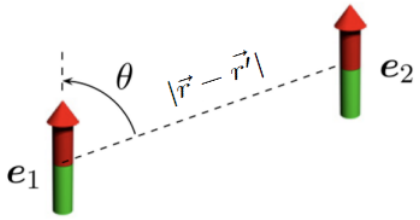

Figure 3.1: Definition of the angle θ. How one can note, the dipolar interaction is anisotropic. The limit alignments, head-to-tail and side by side provide, respectively, the lowest pair interaction energy and the most energetic cost. Figure adapted from [8].

It must be emphasized that there is a competition between interactions of very distinct natures. On one hand, the collisions by contact (first term in the right side of equation (3.2)) are treated by an isotropic and local pseudopotential; on the other hand, the dipolar one (second term on right of (3.2)) is anisotropic and long-ranged. Besides the interplay of this components, the geometry of the trap potential also impacts the stabilization of the system.

The last term inside the bracket in (3.1) is the first quantum fluctuations correction (LHY), introduced by Lee-Huang-Yang in their seminal work [9]. Habitually, this energy contribution is very low due to its dependence with the density raised to three half. However, the LHY correction is able to stabilize systems that interaction balance would conduce to collapse.

In many cases, LHY energy can be neglected, an approach called Mean Field regime. In this description, the interplay of the trapping, contact, and dipolar potentials is enough to bring the ultracold gas to a long-lived BEC in most situations. For example, if $g > 0$ is very large, a cigar trap elongated in the direction of the dipoles favor the head-to-tail orientation, which compensates the high repulsion of the collisions. On the other hand, to $g < 0$, a pancake trap can stabilize the system by maximization of side by side disposition of atoms.

Nonetheless, there are configurations of dipolar gases that quantum fluctuations are indispensable to explain why collapse does not happen. The mechanism behind it lies on an attractive Mean Field contribution in front of a repulsive Beyond Mean Field energy due to large density [?, 3]. In fact, beyond a stable BEC, another phases with unique features have been registered [?]. They will be next described.

3.3 Quantum droplets

At this point, it is introduced the relative magnitude of the dipolar interaction

$$\epsilon_{dd} = \frac{a_{dd}}{a_s} := \frac{C_{dd}m}{12\pi\hbar^2 a_s},$$

which measures how much this term is stronger than contact potential.

When ϵ_{dd} and the number of particles N increase, the dipolar gas is reorganized in a phase denser than the BEC [?, 3]. Even if the trap is switched off, the atomic cloud can remain cohesive. This happens if N is large enough ($> 10^3$ atoms),

when the kinetic energy is not appreciable and interactions dominate [3]. This feature is called "self-boundness", and that configuration is a quantum droplet, a different phase to BECs. The latter can present superfluid features, while the former shows similar properties to ordinary liquids [?, 3].

The most remarkable similarity between dipolar quantum droplets and classical liquids is the density saturation. Whether N increases, the density along the polarization direction will be saturated (see Figure 3.2 a)). This can be interpreted as a sign of low compressibility of dipolar droplets due to the restriction to maintain an effective head-to-tail alignment [?]. This saturation provides to dipolar quantum droplets a flat-top profile. In the center of the arrangement the density is nearly constant, although it decreases rapidly near the boundaries of the droplet, as illustrated in Figure 3.2 b).

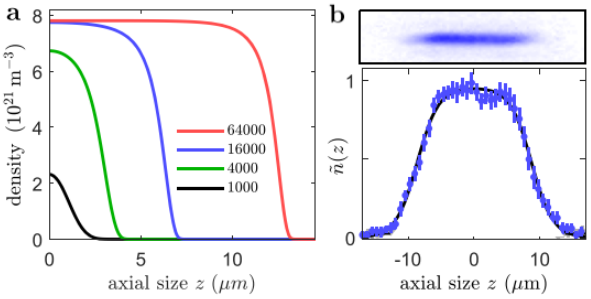

Figure 3.2: Density profile of a quantum droplet through the polarization direction. a) Increasing the number of atoms brings a saturation of density, beyond which the dipolar droplet can only grow rather than become denser. b) Flat-top density pattern. Figure adapted from [?].

The higher density of dipolar quantum droplets in comparison to BECs is explained by Beyond Mean Field effects. In these systems, attractive interactions leaded by dipolar energy overcome the repulsive term. The Mean Field approach predicts a collapse, avoided by quantum fluctuations correction, that arises due to the large density of the configuration. As a consequence, total energy has a minimum at a larger density than that of usual BECs. This energy balance is represented in Figure 3.3.

Hitherto, only an individual quantum droplet arisen from tuning of ϵ_{dd} and N has been considered. However, increasing these parameters ($\epsilon_{dd} > 1$, $N \gtrsim 10^4$) or the confinement in the direction of the dipoles can drive the system to break in many droplets to avoid side by side orientation. In most cases, there is no connection between the droplets

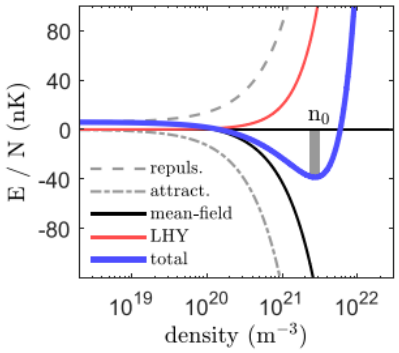

Figure 3.3: In a quantum droplet, the net dipolar attraction (dash-pointed curve) overcomes the repulsion energy provided by contact interaction (dashed curve). Nevertheless, the collapse predicted by Mean Field treatment (black solid curve) does not occur. In contrast, the LHY energy (red curve) becomes relevant as the density increases. The energetic balance (blue curve) point out a density that stabilize the arrangement, where that density is larger than the usual BECs' one. Figure elaborated by [?].

and the density falls to zero between them (See Figure 3.4), which cause loss of coherence, as shown by interference experiments [5].

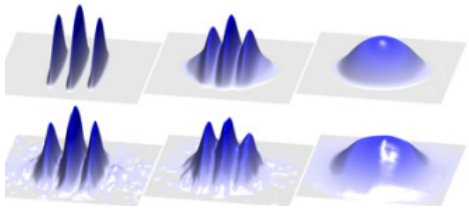

Figure 3.4: Different density aspects of isolated droplets (left), supersolids (center) and BEC (right). The top and bottom lines show the theoretical and observed profiles, respectively. Figure elaborated by [?].

3.4 Supersolids

Even though the transition from a BEC to isolated droplets is the most frequent, a different phase can emerge in a very narrow strip of the parameter space. This phase is characterized by the presence of many dipolar droplets, now connected by a background of non-zero density (Figure 3.4). The droplets are periodically organized, like a solid. Nonetheless, the background has superfluid features, as non-classical rotational inertia [4]. In this phase, every

single atom is simultaneously in the droplets and in the superfluid portion. This provides coherence [3] in addition to both *Diagonal* (typical in solids) and *Off-Diagonal Long Range Orders* (present in superfluids) [4]. This latter dual trait is related to two symmetries broken to originate this phase: continuous translational invariance and gauge one [?, 3].

This character can be verified through excitation spectra. There is a roton mode associated with every symmetry broken [3]. Rotons are elementary excitations identified by a parabolic relation of dispersion (energy-momentum) near the minimum, which is located at a finite value [4]. It manifests as an additional perturbative modulation of density [?]. A transition from BEC to supersolid phase is indicated by splitting of one rotonic mode into two with distinct behaviors. They are originated by the superposition of superfluid and crystal phonons [10].

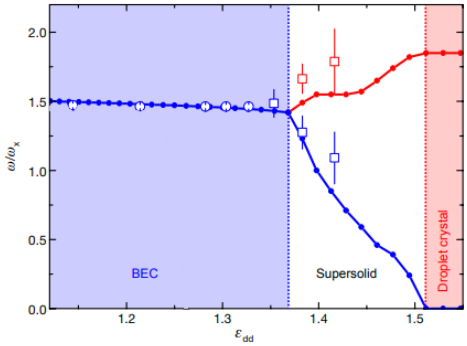

Figure 3.5: Splitting of the quadrupole mode in a supersolid cigar-shaped. Before phase transition, both modes are degenerated in BEC. When ϵ_{dd} crosses the critical value, this degeneracy is lifted and a mode correspondent to solidity arises (red line). It consists of a lattice deformation whose frequency increases as the intensity of dipolar interaction grows. The frequency saturates when isolated droplets arrangement is reached. Contrarily, the other mode corresponds to a compression of superfluid (blue line), which energy decreases until disappears as ϵ_{dd} increases. This occurs due to gain of effective mass. [11]. Solid curves and dots inside them come from Beyond Mean Field calculations. Circular and square dots represent experimental data. Figure adapted from [11].

The lowest-lying excitation is related with superfluid properties. It is composed of out-of-phase oscillations of the background in relation to the crystal arrangement [10], which causes an imbalance in the droplet populations [?, 3]. The correlation between relative displacement and variation of density of the droplets follows the comportment predict by the Beyond Mean Field approach [12].

Conversely, the other mode lifted at phase transition is proper of the solid nature of the regime. In this case, all system oscillates in-phase [10]. The energy associated with this process rapidly increases as ϵ_{dd} overcomes the critical value, which brings this mode to interact and deform the quadrupolar one through avoid-crossing mechanism [?]. The quadrupole mode also suffers splitting in supersolid domain (Figure 3.5). These last excitations are easier to be detected due to their higher energies.

3.5 Thin shell

Spherical shell systems are special owing to they create an extra geometric restriction and accommodate new excitations [1]. This effect arises due to the appearance of a second surface. Shell trapping potential presented in Equation (3.1) is given by [?]

$$V_{tr}(r) = m\omega_0^2 r_0^2 \sqrt{\frac{\left[(r/r_0)^2 - \Delta/\varepsilon\right]^2}{4} + (\Omega/\varepsilon)^2}, \tag{3.3}$$

where $r_0 = 12\pi a_{dd}$ and $\varepsilon = \hbar^2/(mr_0^2)$ are scales of length and energy, respectively, while Δ is the detuning between the dressing radiofrequency and the frequency of resonance and Ω is the Rabi coupling frequency.

This kind of potential is derived from radiofrequency dressing (Figure 3.6). Different bare Zeeman states subjected to a tridimensional magnetic field are coupled by radiofrequency, which is resonant at some positions. This modifies the Hamiltonian of the system and other eigenstates arise. These "dressed states" are now submitted to a new potential with distinct minima [13]. Thus, if the atoms are initially in a single Zeeman state, they tend to migrate to these minima.

When $\Delta = \Omega$, the choice of a large detuning approximates (3.3) by

$$V_{tr}(r) \approx \frac{1}{2} m\omega_0^2 \left(r - R\right)^2,$$

where $R = r_0\sqrt{\Delta/\varepsilon}$ is the maximum of the radial distribution. This means shell becomes a displaced harmonic oscillator around R. If ω_0 is sufficient large to maintain the atoms tightly confined, the spatial restriction imposed by this thin shell in front of the anisotropy of the dipolar interaction provides unique signatures. The most noticeable of them are density profile and elementary excitations, even in the Mean Field regime [1].

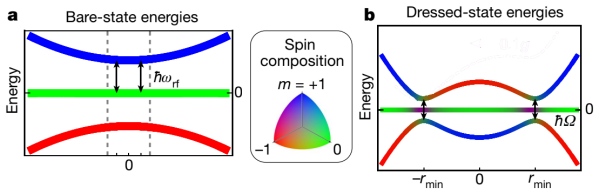

Figure 3.6: Radiofrequency dressing of an one-dimensional system comprising J=1 Zeeman states. a) Bare-states feel the potential proportional to the amplitude of the magnetic field, $B(\vec{r})$. They are coupled by resonant radiofrequency. b) New potentials seen by dressed states. The most energetic one presents minima where the atoms tend to migrate. The three-dimensional equivalent of this confinement is a spherical shell. Figure adapted from [13].

Nevertheless, considering Beyond Mean Field effects is the only way to predict the supersolids in this geometry. Recently, [?] have predicted this phase by numerically solving of eGPE (3.1). They have built a parameter space ϵ_{dd} vs N, which locates the BEC domain, the isolated droplets regime and a very narrow supersolid region (Figure 3.7).

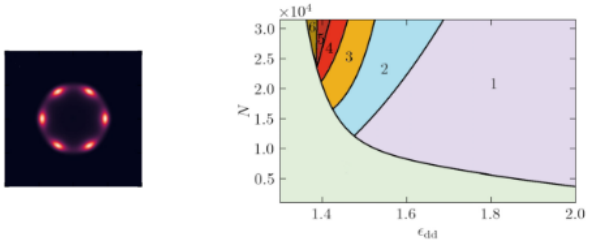

Figure 3.7: On left is shown an equatorial cut of a supersolid bubble-shaped. The polarization axis is crossing the paper plane. It should be noted the denser clusters, where the droplets are placed, and the superfluid background connecting them. On the right, there is a phase diagram of the dipolar thin shell that contains ^{164}Dy atoms. The numbers indicate the quantity of quantum droplets in each region. The one without number is the BEC domain. The narrow range of supersolid occurrence corresponds to numbers 5 and 6. Figure elaborated by [?].

3.6 Our work at IFSC

Our group at IFSC has been working to reach the results achieved by [?] without employing numerical solving. In contrast, the approach is performing semi-analytical calculations of expected value of the Hamiltonian in (3.1) through a proposition of the following *ansatz*. It describes azimuthal modulations with q droplets. The BEC homogeneous state, takes place when $q = 0$. Finally, the domains where BEC, isolated droplets and supersolids have the lowest energy are identified.

$$\psi(\vec{r}) = \sqrt{n_q}\; exp\left[-\frac{1}{2}\left(\frac{r-R}{\sigma}\right)^2\right] exp\left(-\frac{1}{2}\frac{cos^2(\theta)}{\beta^2}\right) \times \times \sum_{p=0}^{q-1} exp\left[-\frac{(\phi - 2\pi p/q)^2}{\alpha^2}\right]. \tag{3.4}$$

We have reproduced the diagram in the direction of ϵ_{dd} (Figure 3.8). Below a critical value, it has been identified a region where BEC dominates ($q = 0$). Transitions from BEC to many isolated droplets has been captured [14]. Emergence of supersolidity is prospected in a narrow region between these both phases due to the overlap of the gaussians' tails inside the sum in (3.4). To confirm it, the superfluid fraction should be evaluated for each configuration [?]. Additionally, as ϵ_{dd} increases with N fixed, the quantity of droplets decreases owing to dipolar interaction.

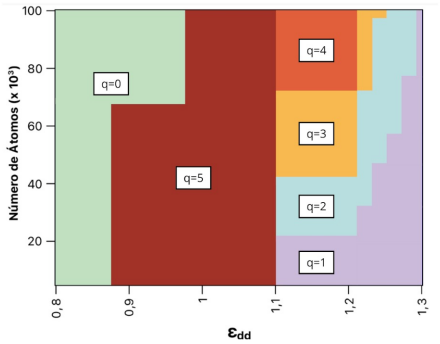

Figure 3.8: Phase diagram built with the ansatz (3.4) [14]. When ϵ_{dd} increases, the system changes from BEC to quantum droplets arrangement and q tends to decrease, as shown by [?]. Conversely, if N grows, q also increases. However, this diagram differs from Figure 3.7 to low N, where numerical solution point out BEC throughout ϵ_{dd} direction. Figure elaborated by [14].

In spite of this partial agreement, the behavior when N varies must be improved. Although for fixed ϵ_{dd} the number of droplets changes more slowly as one moves to right in Figure 3.8, the BEC phase has not been found everywhere for low N. A

hypothesis to explain this is the negligence of the azimuthal component of the kinetic energy in the first calculations. This has been done because that portion is a product between a divergent quantity and another approximately zero. Discarding it undervalues the energy of isolated droplets and supposed supersolids. By regularizing this component of kinetic energy, it might reproduce the domain of BEC in the bottom of the diagram.

3.7 Conclusion

Dipolar ultracold gases display the consequences of the interplay between spatial restriction and interactions of distinct nature. Although the Mean Field regime is frequently succeed, there are situations which its prediction of collapse fails. To obtain a more accurate description, effects of quantum fluctuations must be taken into account. This energy term explains the existence of quantum droplets, an exotic denser phase that shares features with classical liquids, albeit it shows a unique self-bounded character. In sufficiently dense dipolar systems, a lattice of multiple coherent droplets can arises. It constitutes a supersolid, where paradoxically, solid and superfluid properties coexist.

Through an *ansatz*, expected values of the eGPE's Hamiltonian have been calculated to build a phase diagram of a thin shell trapped dipolar system. Our findings agree with a recently carried out numerical solution when the relative strength of dipolar interaction is varied. Nonetheless, we have not reproduced the exclusive occurrence of BEC for low numbers of particles. To achieve it, the discarded azimuthal component of the kinetic energy must be regularized. In our approach, emergence of supersolidity is expected in a narrow region, even though it still needs to be confirmed by evaluating superfluid fraction.

Bibliografia

[1] Diniz, P. C. et al. *Ground state and collective excitations of a dipolar bose-einstein condensate in a bubble trap.* Scientific Reports **10** (2020).

[2] Fabian Böttcher et al. *New states of matter with fine-tuned interactions: quantum droplets and dipolar supersolids* Rep. Prog. Phys. **84**, 012403 (2021).

[3] Lauriane Chomaz et al. *Dipolar physics: a review of experiments with magnetic quantum gases.* Rep. Prog. Phys. **86**, 026401 (2023).

[4] Roccuzzo, S. M. *Supersolidity in a dipolar Bose gas.* Doctoral thesis, University of Trento (2021).

[5] Wenzel et al. *Striped states in a many-body system of tilted dipoles.* Phys. Rev. A **96**, 053630 (2017).

[6] Sánchez-Baena, J.; Bombin, R.; Boronat, J. Ring solids and supersolids in spherical shell-shaped dipolar bose-einstein condensates. Phys. Rev. Res. **6**, 3 (2024).

[7] S. Stringari L. P. Pitaevskii. *Bose-Einstein Condensation.* Oxford University Press (2003).

[8] T Lahaye et al. *The physics of dipolar bosonic quantum gases.* Rep. Prog. Phys. **72**, 126401 (2009).

[9] Lee, T. D., Huang, K., Yang, C. N. *Eigenvalues and Eigenfunctions of a Bose System of Hard Spheres and Its Low-Temperature Properties.* Phys. Rev. **106**, 6 (1957).

[10] Hetkorn, J. et al. *Fate of the Amplitude Mode in a Trapped Dipolar Supersolid.* Phys. Rev. Lett. **123**, 193002 (2019).

[11] Tanzi, L. et al. *Supersolid symmetry breaking from compressional oscillations in a dipolar quantum gas.* Nature. **574**, 382 (2019).

[12] Guo, M. et al. *The low-energy Goldstone mode in a trapped dipolar supersolid.* Nature. **574**, 386 (2019).

[13] Carollo R. A. et al. *Observation of ultracold atomic bubbles in orbital microgravity.* Nature. **606**, 281 (2022).

[14] Yelisetty, Karla M. de C. *Investigação de estado super-sólido em cascas esféricas dipolares finas.* Bachelor thesis, Physics Institute of São Carlos, University of São Paulo (2024).